Crystal and Magnetic Structures of the Mn^{3+} Orbital Ordered Manganite $YBaMn_2O_{5.5}$

Cristian Perca,[†] Loreynne Pinsard-Gaudart,*[,†] Aziz Daoud-Aladine,[‡] María Teresa Fernández-Díaz,[§] and Juan Rodríguez-Carvajal[||]

Laboratoire de Physico-Chimie de l'Etat Solide, Université de Paris Sud, Bât. 414, 91405 Orsay Cedex, France, Laboratory for Neutron Scattering ETH/PSI, Paul Scherrer Institut, CH-5232 Villigen, Switzerland, Institut Laue-Langevin, BP 156, 38042 Grenoble Cedex, France, and Laboratoire Léon Brillouin (CEA-CNRS), CEA/Saclay, 91191 Gif sur Yvette Cedex, France

Received October 27, 2004. Revised Manuscript Received January 14, 2005

The compound $YBaMn_2O_{5.5}$, having only Mn^{3+}, has been prepared by carefully oxidizing/reducing $YBaMn_2O_5/YBaMn_2O_6$. We have determined its crystal (*Icma*, $a \approx 8.161$, $b \approx 7.546$, $c \approx 15.279$ Å) and magnetic (collinear antiferromagnetic) structures using neutron powder diffraction as a function of temperature. The compound is an insulator at all measured temperatures, showing an activated conductivity, $E_a \approx 0.22$ eV. According to bond valence calculations, two Jahn−Teller distorted Mn^{3+} are associated with MnO_6 octahedra and MnO_5 pyramids. The signs of the exchange interactions deduced from the corresponding orbital ordering are in good agreement with the observed magnetic structure. The magnetic moment, at low temperature, of the two kinds of Mn^{3+} ions are slightly different: 3.5(1) μB for the pyramidal site and 3.7(1) μB for the octahedral site. The reduction with respect to the expected moment is due to a combination of covalence and zero-point fluctuations of the AF structure.

1. Introduction

The discovery of the colossal magnetoresistance in manganese oxide perovskites ($AMnO_3$) of general formula $R_{1-x}D_xMnO_3$ (R = trivalent rare earth cations, D = divalent cations such as Ca, Sr, Ba, Pb,...)[1−4] has recently attracted the focus of many research efforts to understand and improve their properties. By changing the D-cation and/or the doping level, one can tune their physical properties from ferromagnetic (F) conductors to antiferromagnetic (AF) insulators. For a large average radius of the A-site ($\langle r_A \rangle$) the conduction band is broad and the material has, in general, a metallic-like behavior. This is usually explained by the double exchange mechanism.[5] If $\langle r_A \rangle$ is small enough the conduction band is narrow, leading to a localization of the charge carriers on specific atomic sites. In some cases the localization occurs in a spatially ordered way. This phenomenon is called charge ordering (CO) and it is accompanied by an increase of the resistivity. Goodenough,[6] using super-exchange theory, and stressing the role of the Jahn−Teller effect on Mn^{3+}, was the first to propose a model explaining qualitatively the magnetic structure of $LaMnO_3$. Combining these concepts with a specific charge and orbital ordering he was able to provide an explanation for the low temperature observations in half-doped ($x = 1/2$) manganites. Recently, Daoud-Aladine et al.[7] have proposed an alternative model in which the electrons localize in regions formed by Mn−O−Mn ferromagnetic pairs (Zener polarons), which are stabilized by a local double exchange mechanism and a structural distortion. To test different hypotheses about the nature of the CO/OO transitions new compounds have to be studied in both mixed and integer valence materials. To overcome the disorder in the A-site of the Mn perovskites we are exploring new compounds presenting well ordered structures. The present paper describes a particular compound within the context described above.

Chapman et al.[8] and McAllister et al.[9] reported the synthesis of a new oxygen deficient manganese perovskite $YBaMn_2O_5$ in which, because of the difference in the radii of the two cations on the A site, Y and Ba order on alternating (001) planes of the perovskite structure. The cited authors solved the structure in the space group *P*4/*mmm*, but later Millange et al.[10] showed that, in fact, the compound crystallizes in the space group *P*4/*nmm*, which is the same as that of $LaBaMn_2O_5$.[11] The structure consists of pyramidal

* To whom correspondence should be addressed. E-mail: loreynne.pinsard@lpces.u-psud.fr.
[†] Université de Paris Sud.
[‡] Paul Scherrer Institut.
[§] Institut Laue-Langevin.
[||] Laboratoire Léon Brillouin (CEA-CNRS).

(1) Von Helmolt, R.; Wecker, J.; Holzapfel, B.; Schultz, L.; Samwer, K. *Phys. Rev. Lett.* **1993**, *71*, 2331.
(2) Chahara, K.; Ohno, T.; Kasai, M.; Kozono, Y. *Appl. Phys. Lett.* **1993**, *63*, 1990.
(3) McCormack, M., Jin, S.; Tiefel, T. H.; Fleming, R. M.; Phillips, J. M.; Ramesh, R. *Appl. Phys. Lett.* **1994**, *64*, 3045.
(4) Mahesh, R.; Mahendiran, R.; Raychaudhuri, A. K.; Rao, C. N. R. *J. Solid. State Chem.* **1995**, *114*, 297.
(5) Zener, C. *Phys. Rev.* **1951**, *81*, 440.
(6) Goodenough, J. B. *Phys. Rev.* **1955**, *100*, 564.
(7) Daoud-Aladine, A. Rodríguez-Carvajal, J.; Pinsard-Gaudart, L.; Fernández-Díaz, M. T.; Revcolevschi, A. *Phys. Rev. Lett.* **2002**, *89*, 097205. See also Zhou, J.-S.; Goodenough, J. B. *Phys. Rev. B* **2000** *62*, 3834.
(8) Chapman, J. P.; Attfield, J. P.; Molgg, M.; Friend, C. M.; Beales, T. P. *Angew. Chem., Int. Ed. Engl.* **1996**, *21*, 108.
(9) McAllister, J. A.; Attfield, J. P. *J. Matter. Chem.* **1998**, *8*, 1291.
(10) Millange, F.; Suard, E.; Caignaert, V.; Raveau, B. *Mater. Res. Bull.* **1999**, *34*, 1.
(11) Millange, F.; Caignaert, V.; Domengès, B.; Raveau, B.; Suard, E. *Chem. Mater.* **1998**, *10*, 1974.

10.1021/cm048119k CCC: $30.25
Published on Web 03/10/2005

manganese layers, sandwiched between alternating Y oxygen-free layers and Ba oxygen-filled layers. A Mn^{2+}/Mn^{3+} charge ordering is observed in this compound.[10] By low-temperature oxygenation it is, in principle, possible to obtain mixed valence compounds of formula $YBaMn_2O_{5+\delta}$ so that it is expected to have Mn^{2+}/Mn^{3+} for $\delta < 0.5$ and Mn^{3+}/Mn^{4+} for $\delta > 0.5$. In practice it is quite easy to obtain the fully oxygenated stoichiometric phase $YBaMn_2O_6$, corresponding to a half-doped manganite. The structure of this compound is far more complex compared to that of $LaBaMn_2O_6$, which crystallizes in the tetragonal space group *P*4/*mmm*.[11] The two reports[12,13] on the crystal structure at room temperature (RT) of $RBaMn_2O_6$ (R═Tb, Y, respectively) are contradictory. We have yet another model, closer to that of reference 12, in which, similarly to the A-site disordered half-doped manganites,[7] Mn^{3+}/Mn^{4+} CO is not as obvious as is Mn^{2+}/Mn^{3+} CO in $YBaMn_2O_5$. This will be published elsewhere.[14] Caignaert et al.[15] have synthesized, by topotactic reaction on a controlled oxygen pressure, a compound with an intermediate oxygen stoichiometry $LaBaMn_2O_{5.5}$ in which Mn ions are purely Mn^{3+}. This compound crystallizes in the space group *Ammm*, and its structure consists of alternating rows of octahedral and pyramidal manganese along the [100] direction. Because of the ordering of the extra oxygen anions, the cell is a superstructure ($a_p \times 2a_p \times 4a_p$) of the elementary perovskite cell. Recently, a report on the $YBaMn_2O_{5.5}$ has been published by Karppinen et al.[16] These authors claim that it has the same structure as its homologous with lanthanum. The present study of $YBaMn_2O_{5.5}$ reveals that the structure in ref 16 is not correct. There are some changes in the crystal structure with respect to $LaBaMn_2O_{5.5}$ that are intimately related to the smaller radius of the Y^{3+} cation, giving rise to a superstructure of the type ($2a_p \times 2a_p \times 4a_p$).

In the present paper we present the synthesis, by topotactic reaction, of the oxygen-deficient manganese perovskite $YBaMn_2O_{5.5}$, which is in fact a stoichiometric compound that can be formulated as $Y_2Ba_2Mn_4O_{11}$, and a study of its crystallographic, magnetic, and transport properties.

2. Experimental Section

To obtain the A-site ordered manganese perovskites $YBaMn_2O_{5+\delta}$ the synthesis must be done in a low oxygen partial pressure atmosphere. We have achieved this by purifying the standard Ar gas with a $p_{O2} = 5 \times 10^{-5}$ bar, by passing it over a Ti−Zr alloy heated at 850 °C.

$$Ti - Zr + 2O_2 \rightarrow TiO_2 + ZrO_2$$

This alloy acts as an oxygen-getter irreversibly forming very stable oxides TiO_2 and ZrO_2. The precursors Y_2O_3, $BaCO_3$, and $MnCO_3$ were mixed in stoichiometric proportion, thoroughly ground, pressed in a cylindrical pellet, sintered at 1250 °C for 20 h, then slowly cooled in the same atmosphere down to room temperature. Under these conditions, the tetragonal oxygen deficient perovskite, $YBaMn_2O_{5+\delta}$, was obtained with δ close to 0 and a very small trace of an unidentified impurity, indicated by the presence of one reflection ($d \sim 3.05$) Å. This impurity is also present in the compound of ref 16 and can be attributed to Y_2O_3, $BaMnO_{3\pm\delta}$, or more complex unknown compounds. The weakness of the reflection, and the absence of further reflections, prevents the unambiguous determination of the nature of the parasitic phase-(s). The fully oxygenated sample was obtained by annealing the reduced one at 500 °C under air for 48 h. To find the best experimental conditions for the synthesis of the phase with an intermediate oxygen content, $YBaMn_2O_{5.5}$, we have studied the behavior of the compounds with $\delta = 0$ and 1, under Ar atmosphere ($p_{O2} = 5 \times 10^{-5}$ bar). Powder samples weighing about 50 mg were heated with a constant rate of 2 °C/min under a gas flow of 10 L/min until 1100 °C in a thermobalance.

The purity checking of the synthesized samples was done with a good-resolution laboratory X-ray diffractometer PAnalytical X'Pert System, equipped with a position-sensitive detector and using Cu $K\alpha_1$ radiation. The crystallographic study was done through Rietveld refinement using the program FullProf[17] on combined X-ray and neutron diffraction data. The RT neutron powder diffraction measurements were obtained at the Institute Laue-Langevin (Grenoble, France) on the diffractometer D1A, using neutrons with wavelength $\lambda = 1.910$ Å, and at Léon Brillouin Laboratory (LLB, Saclay, France) on the diffractometer 3T2 using neutrons of $\lambda = 1.225$ Å. We also used the diffractometer G4.1 ($\lambda = 2.43$ Å) at LLB to study the behavior of the crystal structure, and to determine the magnetic structure, between 1.5 and 300 K.

DC susceptibility and magnetic measurement were performed in the range 4−340 K, with a SQUID magnetometer Quantum Design MPMS 5, in a low field (1000 G) by increasing the temperature after the sample was either zero-field cooled (ZFC) or field-cooled (FC).

The thermogravimetric (TG) analyses were performed with a Setaram TG-DTA 92 thermobalance under different atmospheres. The oxygen content of the samples was determined by thermal analysis measurement. The compound was oxidized in air and for the reference in the calculation we have taken the fully oxygenated formula $YBaMn_2O_6$.

Resistivity measurements were performed between 250 and 450 K on a parallelepipedic pellet of approximate dimensions 1 × 2 × 5 mm using the standard four-point method.

3. Results and Discussions

3.1 Thermal Analysis. The synthesis of the A-site ordered oxygen-deficient perovskite $YBaMn_2O_{5+\delta}$, using a very pure Ar atmosphere, gives good and reproducible results. The sample thus obtained was used in the following for the topotactic synthesis of the compound $YBaMn_2O_{5.5}$. Since the air oxidation starts at 523 K we have first tried to stop the heating slightly just above the oxidation starting temperature, but the result was always the fully oxidized sample. To hinder the complete oxidation we have used argon gas having an effective oxygen partial pressure $p_{O2} = 5 \times 10^{-5}$ bar. The thermogravimetric measurement, shown in Figure 1, under Ar gas flow of 10 L/min with a heating rate of 2 °C/min

(12) Williams, A. J.; Attfield, J. P. *Phys. Rev. B.* **2002**, *66*, 220405R.
(13) Nakajima, T.; Kageyama, H.; Ichihara, M.; Okoyama, K.; Yoshizawa, H.; Ueda, Y. *J. Solid State Chem.* **2004**, *177*, 987.
(14) Pinsard-Gaudart, L.; Perca, C.; Daoud-Aladine, A.; Fernández-Díaz, M. T.; Rodríguez-Carvajal, J., to be published.
(15) Caignaert, V.; Millange, F.; Domengès, B.; Raveau, B.; Suard, E. *Chem. Mater.* **1999**, *11*, 930.
(16) Karppinen, M.; Okamoto, M.; Fjellvag, H.; Motohashi, T., Yamauchi, H. *J. Solid State Chem.* **2004**, *177*, 2122.
(17) Rodríguez-Carvajal, J. *Physica B* **1993**, *192*, 55. For a more recent version see Rodríguez-Carvajal, J. *Recent Developments of the Program FULLPROF*, in *CPD Newsletter* **2001**, *26*, 12 (available at http://journals.iucr.org/iucr-top/comm/cpd/Newsletters/). The program can be obtained from the ftp-site: ftp://ftp.cea.fr/pub/llb/divers/fullprof.2k.

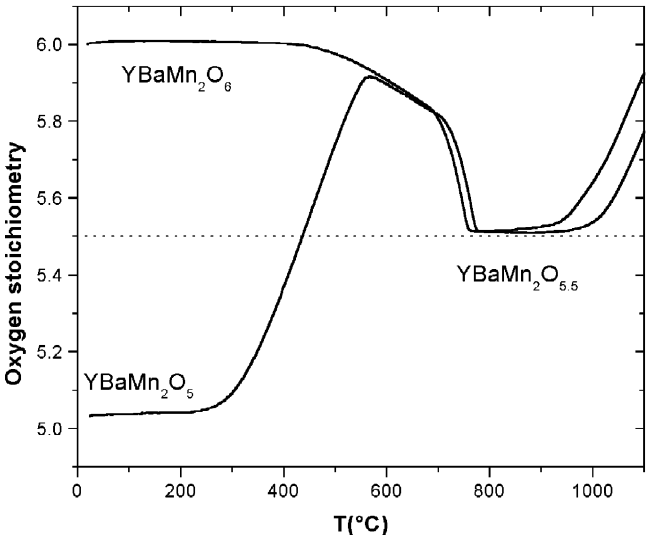

Figure 1. TGA oxygen control of $YBaMn_2O_{5+\delta}$ compounds in an Ar flow of 10 L/min.

shows a plateau, corresponding to the composition $YBaMn_2O_{5.5}$. At low temperature, before reaching the plateau, the oxidation continues beyond $\delta = 0.5$, but as the temperature increases the compound starts to lose weight, reaching a plateau at 1038 K. Further increasing the temperature above 1223 K the sample starts to get weight by decomposing to $YMnO_{3-\delta}$ and $BaMnO_{2.5+\delta}$. As we can see in the same figure, the same result is obtained if we start from $YBaMn_2O_6$. The reduction starts at 708 K, and at 923 K the rate of the weight loss increases, so we can say it is a pseudo-two-step reaction. X-ray diffraction measurements show the same results for the cell parameters of the resulting $YBaMn_2O_{5.5}$ compound, irrespective to the starting compound. The sample used in this study was synthesized starting from $YBaMn_2O_{5+\delta}$ (δ close to 0) and its stoichiometry was found to be $YBaMn_2O_{5.54}$ using thermogravimetric analysis. The refinement of the occupation of the oxygen in the interstitial site (see below) gave a similar result, $YBaMn_2O_{5.55(\pm 0.01)}$, within the experimental error.

3.2 Macroscopic Magnetic and Transport Properties. The temperature dependence of the susceptibility measured at a field of 1000 G with zero-field-cooled (ZFC) and field-cooled (FC) protocols is shown in Figure 2. The curves present two transitions: one at 140 K, which coincides with the irreversibility point in the ZFC−FC measurements and another one at 43 K. The decrease of the susceptibility on the ZFC curve and the irreversibility of the ZFC−FC measurements indicate that the transition at 140 K corresponds to the AF Néel transition (T_N). The same conclusion is reached by the low-temperature neutron powder diffraction study (see section 3.4), but with a shift in the transition temperature.

The increase in the magnetization observed in the FC curve, at T_N temperature, indicates the presence of a weak ferromagnetic contribution, intrinsic to the sample. This is compatible with the symmetry analysis (see next section) which reveals the possibility of a ferromagnetic component, even though only the AF components were observed directly in the neutron diffraction study. The transition observed in the susceptibility curves at around 43 K is due to a parasitic phase that must also have a ferromagnetic component.

The fit of the χ^{-1} versus T curve, measured at a field of 1000 G, in the paramagnetic region, gave an effective magnetic moment per manganese cation of 5.42 μ_B that is larger than the expected spin only value of 4.90 μ_B. This difference could be due to the presence of impurities or to the observed slight departure from stoichiometry (see below). Another possible explanation is that the temperature range is not large enough to get a proper value of the true paramagnetic moment.

Anomalously high values for the effective magnetic moment have also been found in other similar compounds, one of the most studied being $LaMnO_3$, where, even for the stoichiometric composition, Töpfer and Goodenough[18] found a value of 5.55 μ_B, instead of the spin only value of 4.9 μ_B. We expect in the case of $YBaMn_2O_{5.5}$ a similar overestimation of the magnetic moment, either intrinsically to the stoichiometric compound or induced by the small oxygen excess (or both), that could occur and give the small ferromagnetic contribution below T_N. Indeed, the fact that the oxygen stoichiometry is 5.54 has the same consequences as the doping with divalent cations in $LaMnO_3$, leading to the presence of some Mn^{4+} cations. This implies that local Zener polarons[7] or, in general, double exchange ferromagnetic correlations, exist well above the Néel temperature distorting the normal Curie−Weiss paramagnetic region.

The temperature dependence of the resistivity in the paramagnetic region is presented in Figure 3. As we can see from the $\ln\rho = f(1/T)$ linear fit, the resistivity shows insulator-like activated transport, with an activation energy E_a of 0.22 eV. The value of the activation energy is comparable with the energy found by Mahendiran[19] in $La_{1-\delta}Mn_{1-\delta}O_3$ for $\delta = 0.02$ (0.24 eV), but the value of the pre-factor is much larger.

3.3 Crystal Structure at Room Temperature. To solve the structure of the obtained compound we tried a whole X-ray pattern fitting starting from the cell parameters of $LaBaMn_2O_{5.5}$[15] ($a = 3.856$ Å, $b = 8.188$ Å, $c = 15.473$ Å), in the space group *Ammm*. After refinement of the cell parameters, we noticed the presence of few nonnegligible reflections that were not fitted by the *Ammm* model. These reflections were neglected (except for the peak at d ≈ 3.05 Å) or considered as impurity lines in ref 16. The same situation was encountered in the neutron powder diffraction patterns. We found that the extra reflections can be indexed by doubling the *a*-cell parameter, giving an orthorhombic supercell $2a_p \times 2a_p \times 4a_p$.

A careful analysis of the whole pattern fit, without structural model, using the holohedral space group *Pmmm* provided the following presence conditions for the Bragg reflections *hkl*: $h + k + l = 2n$, *h*0*l*: h, $l = 2n$, *hk*0: $h, k = 2n$. These conditions are compatible with the body-centered space groups *I*2*cb* (No. 45, standard setting *Iba*2) and *Imcb* (No. 72, standard setting *Ibam*) in the International

(18) Töpfer, J.; Goodenough, J. B. *J. Solid. State. Chem.* **1997**, *130*, 117−128.
(19) Mahendiran, R.; Tiwary, S. K.; Raychaudhuri, A. K.; Ramakrishnan, T. V.; Mahesh, R.; Rangavittal, N.; Rao, C. N. R. *Phys. Rev. B* **1996**, *53*, 3348.

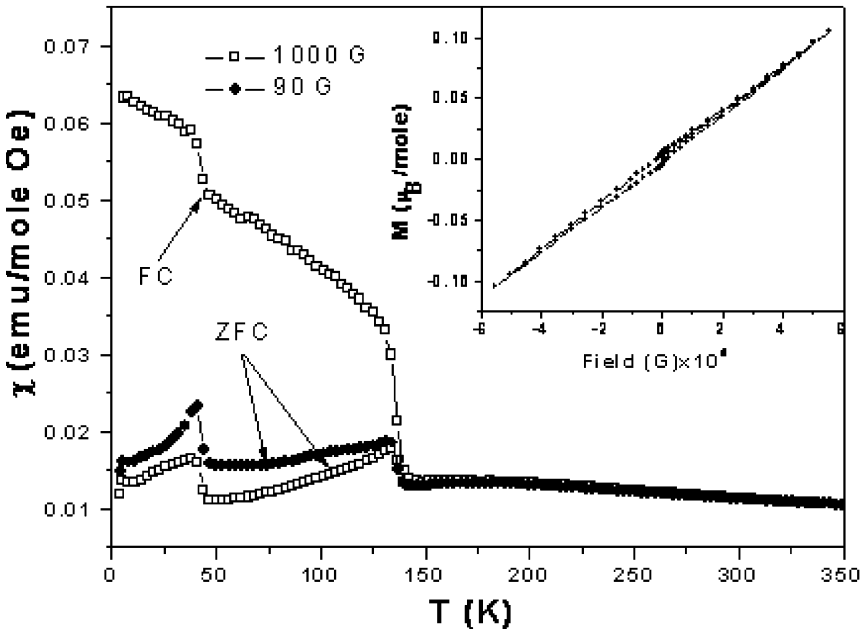

Figure 2. Temperature dependence of the magnetic susceptibility, FC and ZFC, for two different applied fields. The hysteresis loop at 120 K is shown in the inset.

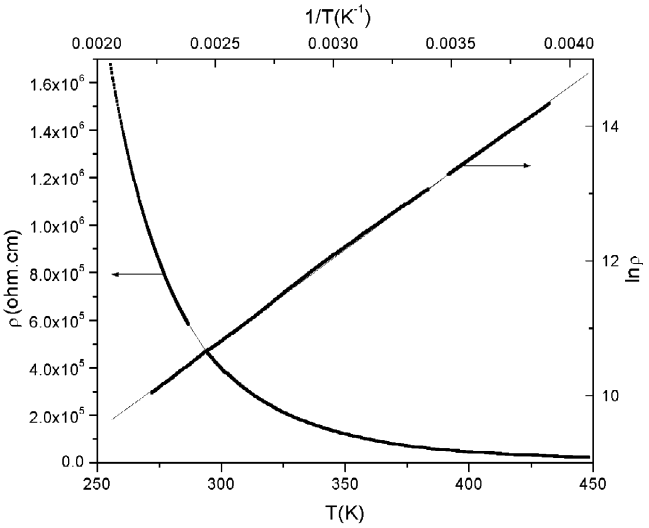

Figure 3. Temperature dependence of the resistivity and the linear plot of the $\ln\rho(1/T)$.

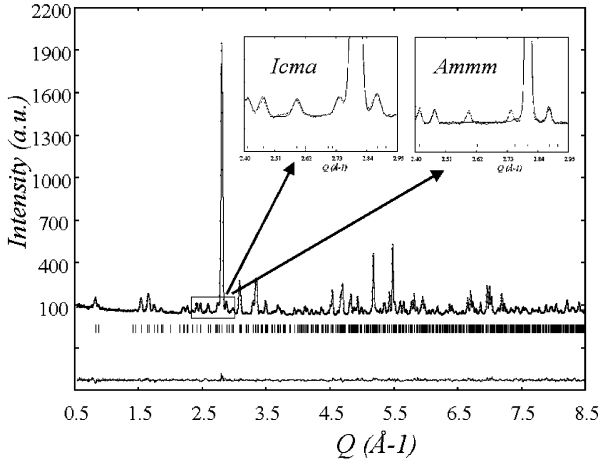

Figure 4. Rietveld refinement of the neutron diffraction data, collected on 3T2, of the $Y_2Ba_2Mn_4O_{11}$ compound. The left inset is a selected area from one of the regions presenting unindexed reflections using the structural parameters of $LaBaMn_2O_{5.5}$. The global plot and the right inset correspond to refinement using the model proposed in the text.

Tables of Crystallography. We decided to change the original setting by conserving the long *c*-axis, perpendicular to the Y/Ba layers, and interchanging the **a** and **b** axes, so the symbols of the two possible space groups become *Ic*2*a* and *Icma*, respectively.

Because the synthesis was done at a rather low temperature, we can suppose that the Y and Ba layers stacking is preserved, the only modification being the oxygen content of the sample and a possible ordering of the manganese octahedra and pyramids. Starting from these observations, we built approximate models compatible with these space groups and we started the refinement. We used the combined data of three independent diffraction patterns at room temperature: one X-ray and two neutron powder patterns. This technique has the advantage of ensuring, at the same time, a good precision in the determination of the cell parameters from the X-ray pattern, and the determination of the oxygen positions and thermal parameters from the neutron patterns. We tried refining the data in both space groups *Ic*2*a* and *Icma*. Since the refinement with the noncentrosymmetric space group did not improve the refinement and it was slightly unstable, we selected the centrosymmetric space group *Icma* that gives quite satisfactory results.

The refinement of all structural and profile parameters in this space group converged rapidly. Figure 4 shows the resulting Rietveld refinement plot of the neutron pattern measured with the instrument 3T2. The obtained atomic coordinates, isotropic thermal parameters, and occupation factors are listed in Table 1 and the agreement factors are provided in Table 2. The excess of oxygen, represented by O6 in Table 1, is negligible and will not be considered for our discussion. A list of selected interatomic distances, Mn−O−Mn angles and bond valence sums calculation for the cations, using the parameters given by Brown,[20] are shown in Table 3.

Table 1. Structural Parameters for $YbaMn_2O_{5.5}$ at Room Temperature as Refined with Combined X-ray and Neutron Powder Diffraction Data in the Space Group *Icma*, $Z = 4$, $a = 8.16121(4)$ Å, $b = 7.54638$ (4) Å, $c = 15.27942(7)$ Å[a]

atom	Wyckoff	*x*	*y*	*z*	occupation factor	biso
Y	8j	0.2729(2)	0	0.0047(2)	1	0.68(3)
Ba	8j	0.2535(3)	0	0.2531(2)	1	0.50(2)
Mn1	8f	0	1/4	0.1144(2)	1	0.67(5)
Mn2	8f	0	1/4	0.3767(2)	1	0.61(5)
O1	16k	0.2306(4)	0.2792(3)	0.0984(2)	2	0.78(5)
O2	8f	0	1/4	0.2518(3)	1	0.58(6)
O3	8j	0.0343(6)	0	0.0932(3)	1	0.78(9)
O4	8j	−0.0291(6)	0	0.3844(3)	1	1.49(1)
O5	4b	0	1/4	1/2	0.5	2.28(2)
O6	4a	0	1/4	0	0.05(1)	2.28(2)

[a] The occupation factors are normalized to one formula unit ($YBaMn_2O_{5.5+z}$).

Table 2. Agreement Factors (*R*-factors in %) for the Combined Refinement of the Three Patterns, Fixing the Wavelength of Cu $K\alpha_1$ and Refining the Neutron Wavelengths

instrument	R_{wp}	R_B	R_F	χ^2
XRD ($\lambda = 1.54060$ Å)	10.5	4.69	3.70	10.2
3T2 ($\lambda = 1.2254(7)$ Å)	10.2	5.73	4.77	3.79
D1A ($\lambda = 1.9112(9)$ Å)	14.2	4.77	3.88	1.57

Table 3. Selected Interatomic Distances, Mn−O−Mn Angles, and Bond Valence Sums (BVS)

bond	distance (Å)	multiplicity	bond valence sum (valence units, v.u.)
<Y−O>	2.5487(13)	10	2.69(1)
<Ba−O>	2.9345(11)	12	2.35(7)
Mn1−O1	1.9101(33)	2	
Mn1−O2	2.0991(57)	1	2.98(1)
Mn1−O3	1.9345(12)	2	
Mn2−O1	2.2426(34)	2	3.28(1)
Mn2−O2	1.9084(59)	1	
Mn2−O4	1.9051(7)	2	
Mn2−O5	1.8846(33)	1	

Mn−O−Mn angles (deg.)		oxygen bond valence sum	
Mn1−O1−Mn2	158.9(1)	O1	1.93(1)
Mn1−O2−Mn2	180	O2	2.14(1)
Mn1−O3−Mn1	154.4(5)	O3	1.92(1)
Mn2−O4−Mn2	164.0(3)	O4	2.30(1)
Mn2−O5−Mn2	180	O5	2.15(1)

At first glance the structure is the same as that for $LaBaMn_2O_{5.5}$. Even though the formal oxidation degree of manganese ions is 3+, in the structure there are two different sites: one with a square pyramidal coordination (Mn1) and another one with octahedral coordination (Mn2). In the *ab* plane, the structure consists of rows of manganese octahedra and pyramids parallel to the *b* direction. In the *a* direction the rows are formed of alternating octahedra and pyramids and in the *c* direction the rows consist of alternating pairs of octahedra and pyramids following the site sequence 1−1−2−2−1−1−2−2. The result of this stacking is the presence of tunnels along the *b* direction (Figure 5).

A closer look at the angles and interatomic distances reveals an important difference comparing to $LaBaMn_2O_{5.5}$. As shown in Figure 6a for the La-based compound the Mn−O−Mn angles between neighboring Mn sites in the *ab* plane are all 180° leading to the total absence of polyhedra tilting. The only distortions, occurring in the La compound, are the

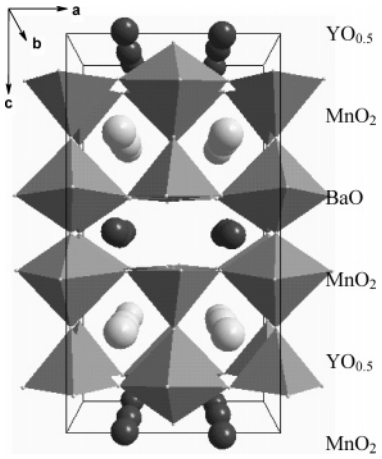

Figure 5. Perspective view of the $YBaMn_2O_{5.5}$ perovskite.

anisotropic Mn−O bond lengths due to the Jahn−Teller effect, and the off-centering of the manganese cations inside the octahedra along the axial direction because of the size mismatch between the La and Ba cations. Figure 6b, for $YBaMn_2O_{5.5}$, shows instead a tilt of the pyramid/octahedron pattern and the Mn−O−Mn angles deviate from the ideal value of 180°. The Mn−O−Mn angle along the *c* direction remains 180°. The tilting of the polyhedra around the [001] axis allows a better accommodation of the small Y^{3+} cation. This tilting is in anti-phase for two consecutive layers, so the corresponding Glazer notation is $\mathbf{a}^0\mathbf{b}^0\mathbf{c}^-$. As we can see in Table 4 the tilting of the polyhedra greatly increases the distortion, Δ, of the coordination environment of A-site cations, especially for Y. The doubling of the **b** cell parameter that we have found experimentally at the beginning of the study, becomes now a natural outcome in the light of these structural findings.

Another important point is the origin of the Mn polyhedra distortions. One of the sources is, as mentioned by Caignaert et al.,[15] the different chemical pressure exerted by the Y and Ba layers, leading to either short or long Mn−O axial distances in the manganese octahedra and pyramids, respectively. This gives also an explanation of the bond valence calculated for the cations in the structure. The small cation Y^{3+} is underbonded (BVS = 2.69 v.u.) and the large cation Ba^{2+} is, consequently, overbonded (BVS = 2.35 v.u.). The Mn1 (pyramidal) is ideally bonded within experimental error (BVS = 2.98 v.u.) whereas the Mn2 (octahedral) is overbonded (BVS = 3.28 v.u.)

The second source of distortion for the case of Mn ions is the electronic structure of the square pyramidal coordinated manganese. By removing one axial ligand from an octahedron, the manganese orbitals pointing toward it will decrease in energy. Thus the d_z^2 orbital, which is pointing exactly in the direction of the leaving ligand, will be the most stabilized. This electronic structure favors the elongation of the axial Mn−O bond type distortion, similar to the Jahn−Teller Q_2 normal mode in octahedral clusters.

The increase in the manganese polyhedra distortion is much smaller compared to that of the A-site cations, because its main origin is the off-centering of the manganese cations along the axial direction toward the Y layer. Taking into account these observations we can now propose the particular

(20) Brown, I. D.; Altermatt, D. *Acta Crystallogr. B* **1985**, *41*, 244.

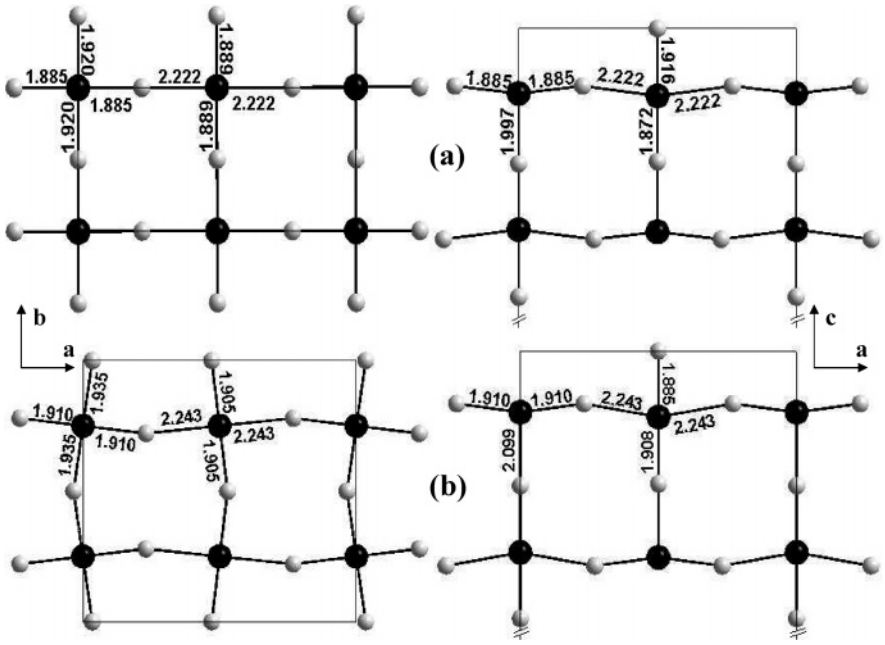

Figure 6. Projections along the [001] direction (left) and [010] direction (right) for $LaBaMn_2O_{5.5}$ (a) and $YBaMn_2O_{5.5}$ (b).

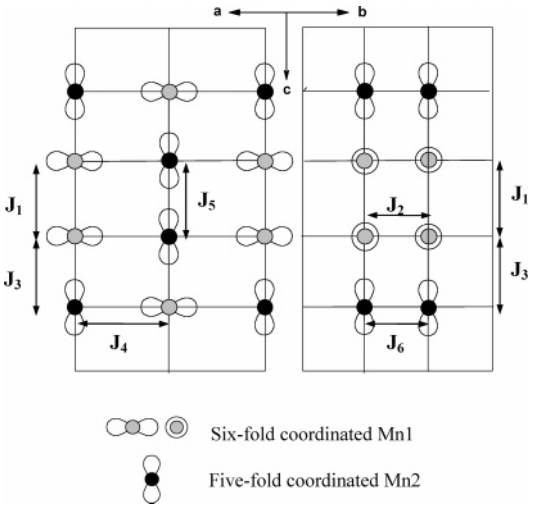

Figure 7. Schematic representation of the orbital order. View along the **b** direction (left) and along the **a** direction (right). The list of the exchange interactions referred in text is also shown.

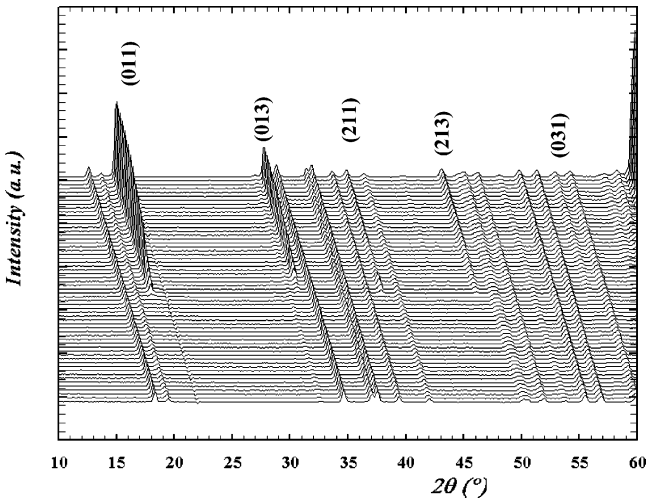

Figure 8. Thermal evolution of the neutron diffraction pattern collected with G4.1 in the temperature range 1.5−290 K. The most important magnetic reflections are indexed using the body-centered crystallographic unit cell.

Table 4. Distortion of the M−O Environment ($\times 10^{-4}$), Where

$$\Delta = \frac{1}{n}\sum_{i=1}^{n}\left(\frac{d_{M-O_i} - \langle d_{M-O}\rangle}{d_{M-O}}\right)$$

$YBaMn_2O_{5.5}$	$LaBaMn_2O_{5.5}$
$\Delta_{Y-O} = 60.4$	$\Delta_{La-O} = 6.3$
$\Delta_{Ba-O} = 40.2$	$\Delta_{Ba-O} = 13.8$
$\Delta_{Mn-O_5} = 13.3$	$\Delta_{Mn-O_5} = 4.5$
$\Delta_{Mn-O6} = 64.1$	$\Delta_{Mn-O6} = 60.8$

orbital ordering stabilized in this type of compounds as that shown in Figure 7. The pyramidal coordinated Mn^{3+} cations have their d_z^2-type orbitals along [001] while the octahedral coordinated Mn^{3+} cations have their d_z^2-type orbitals along [100]. The consequences of this orbital ordering for the exchange interactions will be discussed after describing the magnetic structure.

3.4 Low-Temperature Neutron Diffraction: Magnetic Structure. As discussed in Section 3.2, the magnetic susceptibility measurements show an antiferromagnetic transition at a Néel temperature of $T_N \approx 140$ K. The neutron powder diffraction patterns of $YBaMn_2O_{5.5}$ obtained below the Néel temperature show the presence of magnetic reflections (see Figure 8) that can be indexed by using the propagation vector $\mathbf{k} = (0,0,0)$, so the magnetic cell is identical to the crystallographic cell.

To determine the magnetic structure, symmetry analysis for the space group *Icma* with the propagation vector $\mathbf{k} = (0, 0, 0)$ has been performed for the *8f* position, common to Mn atoms in octahedral and pyramidal coordination. The most important output of the analysis is the complete set of basis functions of the irreducible representations (irreps) classifying the possible magnetic ordering models. The results are summarized in Table 5. We have obtained eight one-dimensional real representations. Four irreps have a single basis function, whereas the other four have two independent basis functions. The refinement of the magnetic

Table 5. Irreducible Representations (Irreps) and Basis Functions of the Space Group *Icma* for the Γ-point, k = (0, 0, 0), and Wyckoff position 8*f*[a]

irreducible representations		Basis Functions Vectors			
		Mn-a	Mn-b	Mn-c	Mn-d
$\Gamma_1(+\,+\,+\,+\,+\,+\,+\,+)$	G_z	(0 0 1)	(0 0 −1)	(0 0 1)	(0 0 −1)
$\Gamma_2(+\,+\,+\,+\,-\,-\,-\,-)$	A_z	(0 0 1)	(0 0 −1)	(0 0 −1)	(0 0 1)
$\Gamma_3(+\,+\,-\,-\,+\,+\,-\,-)$	F_z	(0 0 1)	(0 0 1)	(0 0 1)	(0 0 1)
$\Gamma_4(+\,+\,-\,-\,-\,-\,+\,+)$	C_z	(0 0 1)	(0 0 1)	(0 0 −1)	(0 0 −1)
$\Gamma_5(+\,-\,+\,-\,+\,-\,+\,-)$	F_xG_y	(1 0 0)	(1 0 0)	(1 0 0)	(1 0 0)
		(1 0 0)	(0 1 0)	(1 0 0)	(0 −1 0)
$\Gamma_6(+\,-\,+\,-\,-\,+\,-\,+)$	C_xA_y	(0 1 0)	(0 0 −1)	(0 0 −1)	(0 1 0)
$\Gamma_7(+\,-\,-\,+\,+\,-\,-\,+)$	G_xF_y	(1 0 0)	(−1 0 0)	(0 1 0)	(−1 0 0)
		(0 1 0)	(0 1 0)	(0 1 0)	(0 1 0)
$\Gamma_8(+\,-\,-\,+\,-\,+\,+\,-)$	A_xC_y	(1 0 0)	(−1 0 0)	(−1 0 0)	(1 0 0)
		(0 1 0)	(0 1 0)	(0 0 −1)	(0 −1 0)

[a] Basis functions vectors for the Mn sublattices of the 8*f* site in the following order: Mn-a (0, 1/4, *z*), Mn-b (0, 1/4, 1 − *z*), Mn-c (0, 3/4, *z*), Mn-d (0, 3/4, 1 − *z*), *z* = 0.1144 for Mn1 and z = 0.3767 for Mn2. All representations Γ_i are one dimensional. The characters (+ for 1, − for −1) of each symmetry operator are given in parentheses. The list corresponds to the following ordering of the symmetry operators, in Seitz notation: {1|000}, {2_*z*|0*p*0}, {2_*x*|0*p*0}, {2_*y*|000}, {−1|000}, {*m*_*xy*|0*p*0}, {*m*_*yz*|0*p*0}, {*m*_*xz*|000}, with *p* = 1/2. For the basis functions only the four atoms contained in a primitive cell are needed, the other four atoms (related by the centring translation) have identical basis functions. The symbols F, G, A, and C for labelling the basis functions are conventional notations[24].

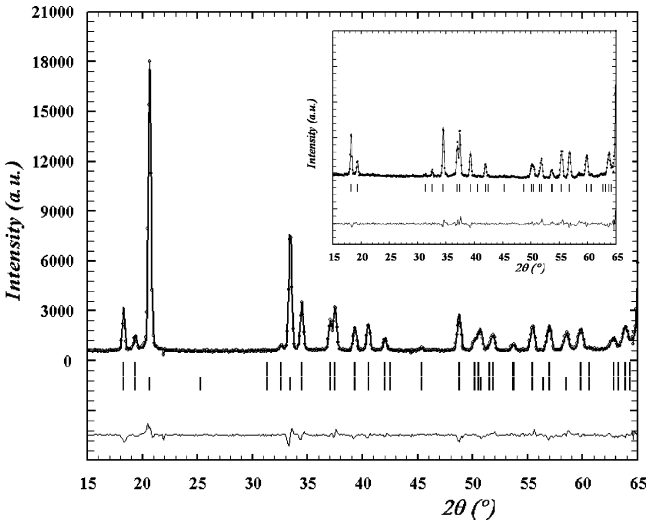

Figure 9. Observed and calculated powder-diffraction patterns of $YBaMn_2O_{5.5}$ at 1.5 K in the low angle part. The inset represents the refinement of the pattern in the paramagnetic state at 280 K for the same angular range without magnetic reflections.

structure at 1.5 K gives the best result with the (G_x, G_x) mode. The two *G* symbols make reference to the spin arrangements (Table 5) on the two Mn sites in the structure. This mode corresponds to the Γ_7 representation. An F_y component is also allowed in the Γ_7 representation. However its amplitude, if different from zero, should be very small and the available data are not of the appropriate quality to get reliable results. In Figure 9 we show the low-angle part of the observed diffraction patterns at 1.5 K collected on G4.1 compared to the calculated pattern by fixing $F_y = 0$. The magnetic moments of the two sites are 3.5(1) μ_B for Mn1 and 3.7(1) μ_B for Mn2, which are reduced with respect to the expected high spin state of 4 μ_B for Mn^{3+}. This could be due to a combination of covalence effects and zero-point fluctuation of the magnetic moments in AF structures. A similar situation is observed in $LaMnO_3$.[21]

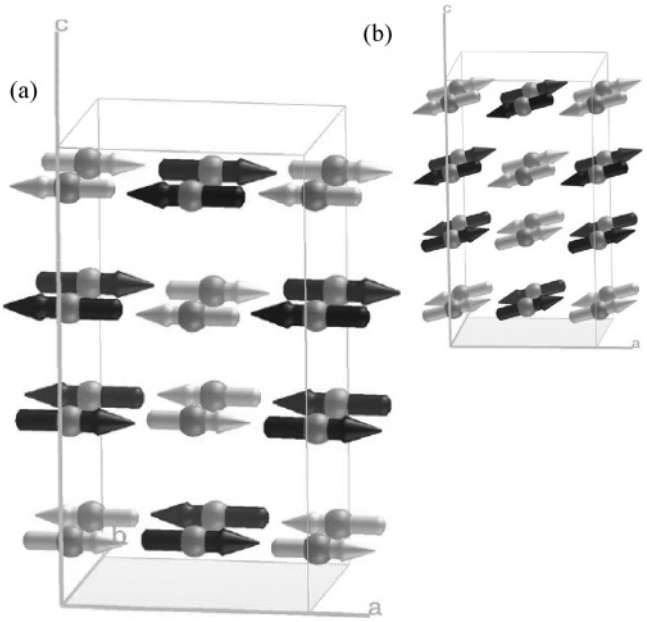

Figure 10. Magnetic structure of $YBaMn_2O_{5.5}$ at 1.5 K (a) and 125 K (b). Mn atoms in octahedral coordination are represented with black arrows. Mn atoms in pyramidal coordination are represented with white arrows.

Figure 10 shows the magnetic structure of $YBaMn_2O_{5.5}$. Looking into the final spin configuration one can verify easily that the magnetic structure of $YBaMn_2O_{5.5}$ is the same as that of $LaBaMn_2O_{5.5}$,[15] which was characterized by a propagation vector **k** = (1/2, 0, 0) but with respect to an orthorhombic cell (***a*** = 3.84 Å, ***b*** = 8.18 Å, ***c*** = 15.42 Å). In our case the *a*-parameter (***b*** in our setting) is doubled, so the propagation vector is **k** = (0, 0, 0).

We performed a sequential refinement to treat all the patterns collected at different temperatures. Due to the low Q-range of the G41 diffractometer, the crystal structure was kept fixed to that obtained at room temperature. Moreover, the magnetic moments of the two manganese atoms, which are very close at *T* = 1.5 K, were constrained to have the same value in the sequential refinements.

An analysis of the results shows that near the transition temperature (*T* ≈ 120 K) two peaks, (211) and (213), were not well fitted with the collinear G_x mode. By mixing the two irreducible representations Γ_1 and Γ_7, the refinements were improved using the G_z (Γ_1) and the G_x (Γ_7) modes. The first ordered state (just below T_N) corresponds therefore to a single collinear (*G*,*G*) = {(G_x, 0, G_z), (G_x, 0, G_z)} mode having components along the *a* and *c* axes.

In Figure 11 the refined value of the Mn magnetic moment has been represented as a function of temperature. The continuous curve has been calculated by using the Brillouin function.

In Figure 12 the thermal evolution of the cell parameters from G41 experiment is shown. The change of the cell parameters above the Néel temperature has a normal positive thermal expansion. It is to be noticed the accident in the curves just at T_N where a change in the slope is observed in all cases. The most important change is that the *a*-parameter exhibits a negative thermal expansion below T_N. This

(21) Moussa, F.; Hennion, M.; Rodríguez-Carvajal, J.; Pinsard, L.; A. Revcolevschi, A. *Phys. Rev. B* **1996**, *54*, 15149.

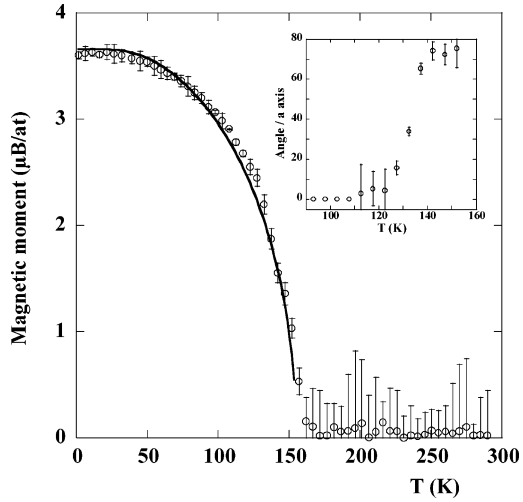

Figure 11. Magnetic moment as a function of temperature. The line corresponds to the calculations using the Brillouin Function. Temperature dependence of the angle between the magnetic component and the *c* axis (inset).

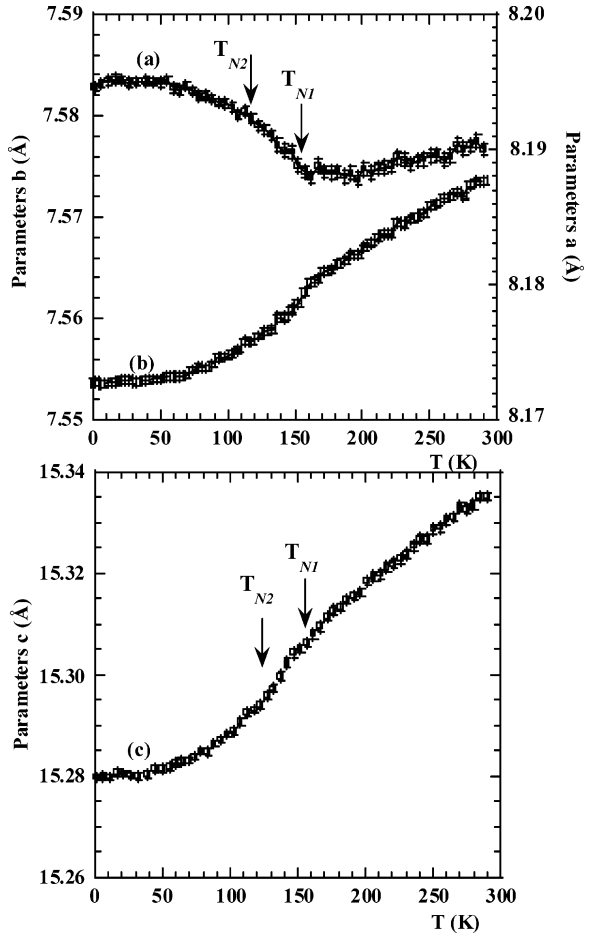

Figure 12. Cell parameters *a*, *b* (upper) and *c* (lower) as a function of temperature.

behavior is clearly related to ordering of the magnetic moment along the *a*-axis as we will show below.

3.5 Origin of the Observed Magnetic Structure: Orbital Ordering. Let us consider the magnetic interactions between the Mn^{3+} ions according to the orbital ordering deduced from the crystal structure (see Figure 7). We shall see that the analysis of the super-exchange paths, and the prediction of the signs of exchange interactions following the Goodenough−Kanamori−Anderson (GKA) rules,[22] is perfectly compatible with the observed magnetic structure.

Table 6. List of Effective Exchange Interactions Considered between Manganese Atoms[a]

interaction	distance (Å)	representative exchange path	angle Mn−O−Mn
J_1	3.4962	Mn1−O3−O3−Mn1	97.78
J_2	3.7732	Mn1−O3−Mn1	154.41
J_3	4.0072	Mn1−O2−Mn2	180
J_4	4.0829	Mn1−O1−Mn2	158.77
J_5	3.7688	Mn2−O5−Mn2	180
J_6	3.7732	Mn2−O4−Mn2	163.85

[a] Bond lengths, representative exchange paths, and relevant exchange angles are given.

In Table 6, we list the effective exchange interactions that should be considered to study the problem. This table and the analysis of the magnetic phase diagram discussed below have been obtained using the method described in reference 23. Considering only first nearest neighbor exchange interactions (maximum distance of 4 Å), we obtain six different exchange interactions to describe the system.

Along the *c* direction, we have two different exchange interactions, J_1 and J_5, coupling two equivalent Mn ions. The exchange interaction J_1 connects two Mn1 ions by a super-super-exchange path (involving two oxygen atoms). Direct exchange between half-filled d_z^2 orbitals through the square face of the pyramids is probably negligible because the distance between the ions is relatively high, so the orbitals involved in the super-super-exchange paths ($d_{x^2-y^2}$) are empty. In any case the interaction should be very small and probably negative (AF interaction, $J_1 < 0$ and $J_1 \approx 0$). The J_5 interaction connects two Mn2 ions by a 180° super-exchange path involving two-half-filled d_z^2 orbitals, so a strong AF-interaction is expected ($J_5 < 0$). There is another interaction, J_3, along *c* but coupling this time Mn1 and Mn2 ions. This interaction involves a half-filled d_z^2 orbital in the Mn1 site with an empty $d_{x^2-y^2}$ orbital in the octahedral Mn2 site. A relatively weak F-interaction ($J_3 > 0$) is then expected.

The interaction J_4 corresponds to the exchange between the Mn1 and Mn2 ions along *a*. According to the orbital ordering shown in Figure 7 we have always half-occupied d_z^2 orbitals linked with empty $d_{x^2-y^2}$ orbitals along *a*. The interaction J_4 is expected to be weak and F ($J_4 > 0$). The two last interactions, J_2 and J_6, connect equivalent manganese atoms, two Mn1 for J_2 and two Mn2 for J_6, along the *b* direction. Only empty $d_{x^2-y^2}$ orbitals (see Figure 7) are linked, so weak AF-interactions are expected ($J_{2,6} < 0$).

Due to the nonfrustrating topology of the discussed model (interactions only for distances lower than 4 Å) the phase diagram is straightforward: it is directly related to the sign of the exchange integrals. We used, however, the method discussed in ref 23 to confirm the predicted characteristics of the phase diagram. To simplify the calculations we considered $J_1 = 0$ and $J_2 = J_6$ that seem reasonable from the

(22) Goodenough, J. B. *Magnetism and the Chemical Bond*; Wiley and Sons: New York, 1963; Chapter III.
(23) El Khayati, N.; Cherkaoui El Moursli, R.; Rodríguez-Carvajal, J.; André, G.; Blanchard, N.; Bourée, F.; Collin, G.; Roisnel, T. *Eur. Phys. J.* **2001**, *B22*, 429. See also Rousse, G.; Rodríguez-Carvajal, J.; Wurm, C.; Masquelier, C. *Solid State Sci.* **2002**, *4*, 973.
(24) Bertaut, E. F. *Acta Crystallogr.* **1968**, *A 24*, 217.

Table 7. Labels of Magnetic Structures and Sign Sequences of Magnetic Moments Corresponding to the Different Mn Atoms Characterizing the Eight Possible Collinear Magnetic Structures for k = (0, 0, 0)[a]

	Sequence of Magnetic Moments								conditions of the interactions for the different magnetic structures
	M_{Mn1a}	M_{Mn1b}	M_{Mn1c}	M_{Mn1d}	M_{Mn2a}	M_{Mn2b}	M_{Mn2c}	M_{Mn2d}	
1(G,-G)	+	−	+	−	−	+	−	+	$J_{2,3,4,5} < 0$
2(A,-A)	+	−	−	+	−	+	+	−	$J_{3,5} < 0$; $J_{2,4} > 0$
3(C,-C)	+	+	−	−	−	−	+	+	$J_{2,3} < 0$; $J_{5,4} > 0$
4(F,-F)	+	+	+	+	−	−	−	−	$J_{3,4} < 0$; $J_{2,5} > 0$
5(G,G)	+	−	+	−	+	−	+	−	$J_{2,5} < 0$; $J_{3,4} > 0$
6(A,A)	+	−	−	+	+	−	−	+	$J_{4,5} < 0$; $J_{2,3} > 0$
7(C,C)	+	+	−	−	+	+	−	−	$J_{2,4} < 0$; $J_{3,5} > 0$
8(F,F)	+	+	+	+	+	+	+	+	$J_{2,3,4,5} > 0$

[a] For calculating the magnetic phase diagram we have considered $J_1 = 0$ and $J_2 = J_6$. The observed magnetic structure corresponds to the sequence of the fifth row and the exchange conditions are consistent with GKA rules.

geometrical features of the exchange paths. There are only eight stable possible magnetic structures with **k** = (0, 0, 0) (Table 7). The magnetic structure experimentally observed for $YBaMn_2O_{5.5}$ is numbered as 5 in Table 7 and it is described by the sequence $(G,G) = (+ - + - + - + -)$.

The conditions to obtain the observed structure as ground state are $J_1 \approx 0$, $J_{2,5} < 0$ and $J_{3,4} > 0$, which are completely compatible with the prediction of the GKA rules for the structure-deduced orbital ordering described above. This leads to a picture of the magnetic structure, identical to that of $LaBaMn_2O_{5.5}$,[15] as a network of parallel ferromagnetic spin-ladders. Each F spin ladder lies along the *a*-axis, in the (010) plane, and it is AF-connected along the *b* and *c* axes to the neighboring ladders (see Figure 10). In the (010) plane, half of the manganese ions of every ladder are connected to adjacent ladders by the Mn2−O−Mn2 AF pathway. Along the [010] direction, all the Mn ions of a ladder are AF-connected to the upper and lower ladders. The anomalous behavior of the *a*-parameter is probably due to a reinforcing of the orbital ordering upon magnetic ordering. As seen in Figure 7, an increasing of the electron density in the d_z^2-like orbitals of MnO_6 octahedra, which are oriented along *a*, produces the observed behavior.

4. Conclusions

In the present study we have shown the synthesis, by topotactic reaction, of the oxygen deficient perovskite $YBaMn_2O_{5.5}$ using controlled oxygenation or de-oxygenation of the completely reduced or the completely oxidized sample, respectively. We have also investigated its magnetic and transport properties as well as its crystal and magnetic structure. On the basis of Rietveld refinement of combined X-ray and two neutron powder diffraction patterns we have shown that a doubling of the cell is present in this case, as compared to the La-based compound, due to a tilting ($a^0b^0c^-$) of the polyhedra around the [001] direction. The existence of two distinct types of Mn^{3+} cations, in square pyramidal and octahedral coordination, leads to the formation of a particular orbital ordering. The signs of the exchange interactions deduced from this type of orbital ordering are consistent with the observed formation of F-ladders along *a*, AF-coupled along *b* and *c* directions, resulting in a global AF structure. Magnetic susceptibility measurements showed additionally a field-dependence of the magnetic moment, probably due to a slightly canted antiferromagnetic structure and/or the presence of an unknown impurity phase. The resistivity measurements have shown an insulator-like activated behavior with a low activated energy, comparable to that of $LaMnO_3$.

Acknowledgment. We thank Prof. P. Berthet, Dr. R. Suryanarayanan, and Prof. N. Dragoe for helpful discussions.

CM048119K